Investigating the effect of drug release on in-stent restenosis: A hybrid continuum - agent-based modelling approach

Computer Methods and Programs in Biomedicine 241 (2023) 107739

Contents lists available at ScienceDirect

Computer Methods and Programs in Biomedicine

journal homepage: www.elsevier.com/locate/cmpb

Investigating the effect of drug release on in-stent restenosis: A hybrid continuum – agent-based modelling approach

Anna Corti [a,1], Alistair McQueen [b,1], Francesco Migliavacca [a], Claudio Chiastra [c], Sean McGinty [b,*]

[a] Laboratory of Biological Structure Mechanics (LaBS), Department of Chemistry, Materials and Chemical Engineering "Giulio Natta", Politecnico di Milano, Milan, Italy
[b] Division of Biomedical Engineering, University of Glasgow, Glasgow, UK
[c] PoliTo[BIO]Med Lab, Department of Mechanical and Aerospace Engineering, Politecnico di Torino, Turin, Italy

ARTICLE INFO

Keywords:
Computational multiscale modelling
Drug transport model
Agent-based model (ABM)
Coronary artery
Percutaneous coronary intervention
Drug-eluting stent

ABSTRACT

Background and objective: In-stent restenosis (ISR) following percutaneous coronary intervention with drug-eluting stent (DES) implantation remains an unresolved issue, with ISR rates up to 10%. The use of anti-proliferative drugs on DESs has significantly reduced ISR. However, a complete knowledge of the mechano-biological processes underlying ISR is still lacking. Multiscale agent-based modelling frameworks, integrating continuum- and agent-based approaches, have recently emerged as promising tools to decipher the mechano-biological events driving ISR at different spatiotemporal scales. However, the integration of sophisticated drug models with an agent-based model (ABM) of ISR has been under-investigated. The aim of the present study was to develop a novel multiscale agent-based modelling framework of ISR following DES implantation.
Methods: The framework consisted of two bi-directionally coupled modules, namely (i) a drug transport module, simulating drug transport through a continuum-based approach, and (ii) a tissue remodelling module, simulating cellular dynamics through an ABM. Receptor saturation (RS), defined as the fraction of target receptors saturated with drug, is used to mediate cellular activities in the ABM, since RS is widely regarded as a measure of drug efficacy. Three studies were performed to investigate different scenarios in terms of drug mass (DM), drug release profiles (RP), coupling schemes and idealized *vs.* patient-specific artery geometries.
Results: The studies demonstrated the versatility of the framework and enabled exploration of the sensitivity to different settings, coupling modalities and geometries. As expected, changes in the DM, RP and coupling schemes illustrated a variation in RS over time, in turn affecting the ABM response. For example, combined small DM – fast RP led to similar ISR degrees as high DM – moderate RP (lumen area reduction of ~13/17% *vs.* ~30% without drug). The use of a patient-specific geometry with non-equally distributed struts resulted in a heterogeneous RS map, but did not remarkably impact the ABM response.
Conclusion: The application to a patient-specific geometry highlights the potential of the framework to address complex realistic scenarios and lays the foundations for future research, including calibration and validation on patient datasets and the investigation of the effects of different plaque composition on the arterial response to DES.

1. Introduction

Coronary artery disease is the leading cause of death worldwide [1]. Treatment typically involves percutaneous coronary intervention with drug-eluting stent (DES) implantation. Despite innovations in stent technology, in-stent restenosis (ISR) remains the most common side-effect [2]. ISR rates of up to 10% are still observed clinically, with complex lesions the primary culprit [2,3]. ISR results from excessive synthetic smooth muscle cell (SMC) proliferation and extracellular matrix (ECM) deposition, initiated by the inflammatory response to vascular injury [4]. Antiproliferative drugs coated on DESs inhibit SMC proliferation and have resulted in reductions in ISR rates. However, a complete understanding of the different biological, mechanical and technical factors that lead to ISR is still lacking [4]. In particular, the

* Corresponding author.
E-mail address: Sean.Mcginty@glasgow.ac.uk (S. McGinty).
[1] The authors contributed equally to this work and share first authorship.

https://doi.org/10.1016/j.cmpb.2023.107739
Received 15 February 2023; Received in revised form 5 July 2023; Accepted 27 July 2023
Available online 1 August 2023

optimal drug delivery strategy has yet to be defined [5].

In-silico investigation provides understanding of the complex mechanisms driving ISR. Recent multiscale agent-based modelling frameworks have emerged as a promising approach to gain insights into the mechanobiological mechanisms underlying vascular adaptation processes, especially restenosis [6]. The suitability to describe the complex network of events and to capture spatial heterogeneity are attractive characteristics of agent-based models (ABMs), enabling simulation of cellular dynamics and mechanobiological mechanisms, involving cell-cell and cell-environment interactions [6]. To the best of the authors' knowledge, a multiscale framework coupling the state-of-the-art drug transport model with an ABM of ISR following DES implantation is lacking. To date, several computational studies focused on modelling either ISR (through a continuum or ABM approach) or drug elution kinetics. However, (i) the ISR studies neglected the effect of drug or considered a simple model of drug delivery (*e.g.*, [7,8]) encompassing only diffusion and ignoring the critical binding processes and (ii) the drug transport models did not consider the concurrent arterial wall remodelling, in turn affecting the drug transport and kinetics [9,10]. Only recently, McQueen et al. [11] proposed a fully-continuum multiscale model of ISR following DES implantation, by explicitly coupling a drug transport model with partial differential equations of cellular dynamics driving arterial wall remodelling and ISR.

The aim of the present work is to contribute to the advancement of *in-silico* modelling of ISR by proposing a multiscale agent-based modelling framework of ISR in coronary arteries that couples continuum-based drug transport simulations with an ABM of cellular dynamics. Moreover, to show the potential utility of the framework, different scenarios are investigated, including the effect of drug mass (DM) and drug release profiles (RP) as well as different framework coupling modalities on ISR in an idealized coronary artery cross-section. Finally, to demonstrate the feasibility of extension to more realistic scenarios, a proof-of-concept application of the framework to a patient-specific coronary artery cross-section is considered.

2. Methods

2.1. Multiscale framework

Fig. 1 shows the multiscale ISR framework, which receives a 2D stented coronary artery cross-section and a literature-derived post-intervention inflammatory curve as input, and generates the artery cross-section configuration at 1-month as output. The framework consists of two coupled modules: (i) drug transport module and (ii) tissue remodelling module. Within the drug transport module, the geometry is meshed and transient simulations of drug transport are performed [11]. Receptor saturation (RS) (fraction of saturated target receptors, a measure of drug efficacy) is computed and passed to the tissue remodelling module, which simulates the 1-month post-intervention remodelling [12–14]. Specifically, a 2D ABM replicates SMC and ECM activities in response to the intervention-induced inflammation and the RS, thus generating the 1-month remodelled arterial configuration. The framework can be executed either as one-way or two-way coupling. One-way coupling involves simulating the drug transport module over 1-month and providing the RS output along the entire period to the tissue remodelling module, which in turn simulates the arterial wall remodelling over 1-month. Differently, with two-way coupling, the drug transport module is run on the initial geometry up to a given coupling time (*e.g.*, 3 days), the RS curve is then passed to the tissue remodelling module, simulating arterial wall remodelling over the same time period, then the drug transport module is run again on the remodelled geometry (output from the tissue remodelling module) over the following coupling period (*e.g.*, from day 3 to day 6): this process continues until the end of the follow-up period (*i.e.*, 1-month in this case).

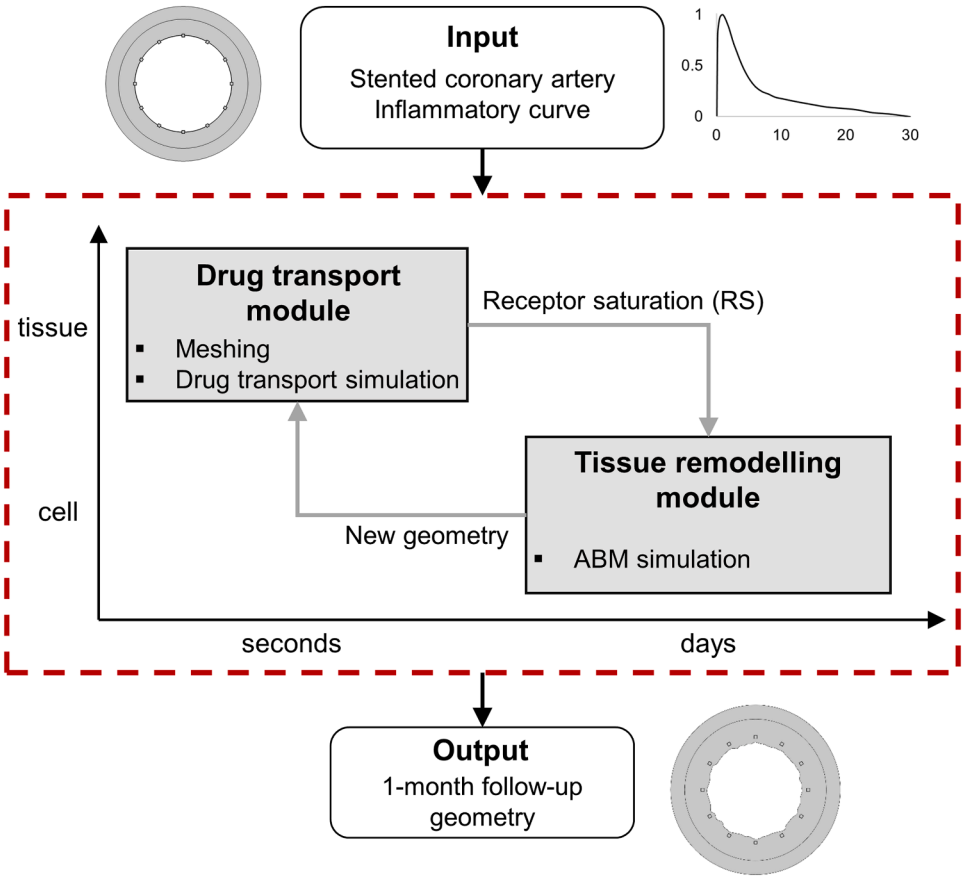

Fig. 1. Multiscale computational agent-based modelling framework. Starting from the stented coronary artery cross-section, the framework (dashed red box) simulates arterial wall remodelling and in-stent restenosis (ISR) over 1-month of follow-up, generating as output the remodelled arterial geometry. The framework consists of two bi-directionally coupled modules, namely (i) the drug transport module at the tissue-seconds scale, in which the artery model is meshed and the drug transport simulation is performed to compute the receptor saturation (RS), and (ii) the tissue remodelling module at the cell-days scale, in which an agent-based model (ABM) simulates cellular activities and arterial wall remodelling in response to the intervention-induced inflammation and the RS, and generates the remodelled arterial configuration.

Both an idealized and a patient-specific coronary artery cross-section were considered (Fig. 2). The idealized stented coronary artery (Fig. 2A), implemented in COMSOL Multiphysics 5.6a (COMSOL AB), possessed a lumen diameter, media (considered as a single layer, embedding the intima layer of 0.01 mm thick) and adventitia thickness of 3 mm, 0.51 mm and 0.4 mm, respectively [9,11]. The Xience Prime DES (Abbott) with 12 equally-spaced square struts of 81 μm thickness, with 8 μm thick polymer coating was half-embedded in the wall. The patient-specific geometry (Fig. 2B) consisted of a cross-section with lumen and stent geometries derived from a three-dimensional patient--specific stented coronary artery reconstructed from post-operative optical coherence tomography images. The patient coronary artery was treated with a 3.5 × 28 mm Xience Prime DES at the Institute of Cardiology, Catholic University of the Sacred Heart (Rome, Italy) [15,16]. The stent presented 18 struts/ring and same strut characteristics of the idealized geometry. The cross-section lumen hydraulic diameter was 3.82 mm and circular 0.65 mm thick media and 0.51 mm thick adventitia layers were defined in accordance with the thickness-diameter ratio of the idealized geometry. In both the idealized and patient-specific geometries, the endothelium was assumed to be completely denuded after stent deployment.

2.1.1. Drug transport module

Transient simulations of drug transport were performed in COMSOL Multiphysics. Fig. 3A presents a schematic of the geometry, with details of the boundaries (Γ) and domains (Ω). Sirolimus transport was modelled as in [10,11,17], being the most widely studied drug in the context of DES [18,19]. Tables 1 and 2 provide the equations defining the drug transport model (with parameters values and references detailed in Supplementary Table 1) and boundary conditions, respectively. Briefly, (i) drug release from a durable coating was modelled as a diffusion process [20], (ii) drug transport within the porous media and adventitia was modelled by coupling Darcy's law with advection-diffusion-reaction equations and (iii) drug retention was considered in the media layer, where nonlinear saturable binding kinetics were implemented to distinguish between drug bound specifically (b^s) to cells and non-specifically (b^{ns}) to non-cellular constituents (*e.g.*, ECM).

A finite element mesh comprising boundary layers and triangular and quadrilateral elements was created in COMSOL Multiphysics (Fig. 3A). A mesh independence study was performed, investigating the impact of mesh size on RS. The selected mesh (~327,000 elements) guaranteed convergence and perturbations in RS below 1%. The implicit backward differentiation formula method was used for the time discretization of the model. The relative and absolute tolerances were set to 10^{-3} and 10^{-4}, respectively.

RS was computed at each time step over the domain. The RS output served as input to the ABM either as RS_{map}, consisting of the spatial contour of RS at a specific time instant, or as RS_{curve}, the time-varying mean RS over space.

It is noted that the Xience stent, upon which the strut geometry in this study is based, in reality delivers everolimus via bi-phasic diffusion kinetics [21]. A single mode of diffusion is considered in this study for simplicity and sirolimus is chosen owing to the availability of parameter values in the literature.

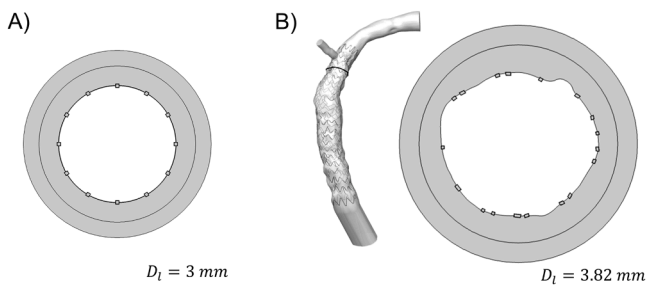

Fig. 2. A) Idealized stented coronary artery cross-section, with lumen diameter $D_l = 3$ mm. B) Patient-specific stented coronary artery cross-section (right), with lumen hydraulic diameter $D_l = 3.82$ mm. The lumen and stent geometries were extracted from the three-dimensional patient arterial model reconstructed from post-operative optical coherence tomography images (left).

2.1.2. Tissue remodelling module

A 2D ABM was implemented in Matlab (MathWorks) to simulate the post-intervention arterial wall remodelling at the cell-tissue scale in response to the intervention-induced inflammation and drug released. The ABM structure relied on previously developed ABMs of restenosis [12–14], adapted to account for a two-layer coronary artery geometry and for the effect of drug. Fig. 3B shows the ABM of the two-layer stented coronary artery cross-sections, composed of media and adventitia layers. The ABM was implemented on a 300 × 300 hexagonal grid and was generated by importing the nodal coordinates from the drug transport module and scaling them by a 25 μm/ABM site scale factor (*i.e.*, 1 cell/ABM site, SMC diameter~25 μm [22]). The media was populated with SMCs and collagen and elastin (named as ECM). The adventitia was populated with fibroblasts and collagen, with layer-specific cell and ECM densities [12–14,23,24].

The ABM was initialized with the inflammatory input (I) and the RS input (RS_{ABM}), driving cellular activities as detailed in Table 3 and explained below. I represented the post-intervention inflammation and was used as the ISR trigger, assuming cellular activity heightened as inflammation increased, potentially leading to intimal hyperplasia and ISR [12–14]. As shown in the Supplementary Fig. S1, I consisted of a time-varying input (with peak around day 3 [25,26], vanishing at day 30) equally influencing all the agents in the media layer (uniform spatial input). RS_{ABM} represented the fraction of SMC binding sites bound to drug and accounted for the inhibitory effect on SMC proliferation. The RS_{ABM} value was assigned to each agent in the media and was derived either from RS_{curve} or RS_{map} provided by the drug transport module. In the case of RS_{curve}, RS_{ABM} was defined by assigning all the medial SMC agents the RS value at the specific ABM time-step. Differently, in the case of RS_{map}, RS_{ABM} was defined by assigning to each medial SMC agents the corresponding RS value at that time-step. However, since RS_{map} obtained from the drug transport module at a specific time was computed on the original geometry, a method to assign RS_{ABM} values to the neointima was implemented in the ABM, such that the RS_{ABM} contour in the neointima radially reflected the RS_{ABM} contour in the media (Supplementary Fig. S2). Overall, the RS_{ABM} input derived from RS_{curve} was uniform in space, while the RS_{ABM} input derived from RS_{map} accounted for spatial RS distribution and heterogeneity.

Cell mitosis/apoptosis and ECM production/degradation were defined such that in the media layer SMC mitosis and ECM production were perturbed by I and RS_{ABM}, while in the adventitia baseline homoeostasis was reproduced. The probability equations governing cell mitosis/apoptosis and ECM production/degradation in the media and adventitia layers are detailed in Table 3, with parameters in Table 4. The formulation of the probability equations relied on previous studies, and in particular on the hypotheses that: (i) baseline dynamics (*i.e.*, in the absence of I and RS_{ABM} inputs) guarantee balanced mitosis/apoptosis as well as ECM production/degradation, thus requiring the introduction of β_{med} and β_{adv} coefficients to compensate the biased favoured ECM degradation, as detailed in [13,23]; (ii) only the media layer (here considered as comprehensive of both intima and media) was actively involved in the restenosis process; (iii) arterial tissue growth was mainly attributable to the perturbation of cell mitosis and ECM production (while potential changes in cell apoptosis and ECM degradation processes were neglected); (iv) the higher the inflammatory response I, the more proliferative and synthetic cellular activities are intensified, as defined in the probability equations of $p^h_{division}$ and $p^h_{ECMproduction}$ in the media detailed in Table 3; (v) RS_{ABM} accounts for the cytostatic effect of

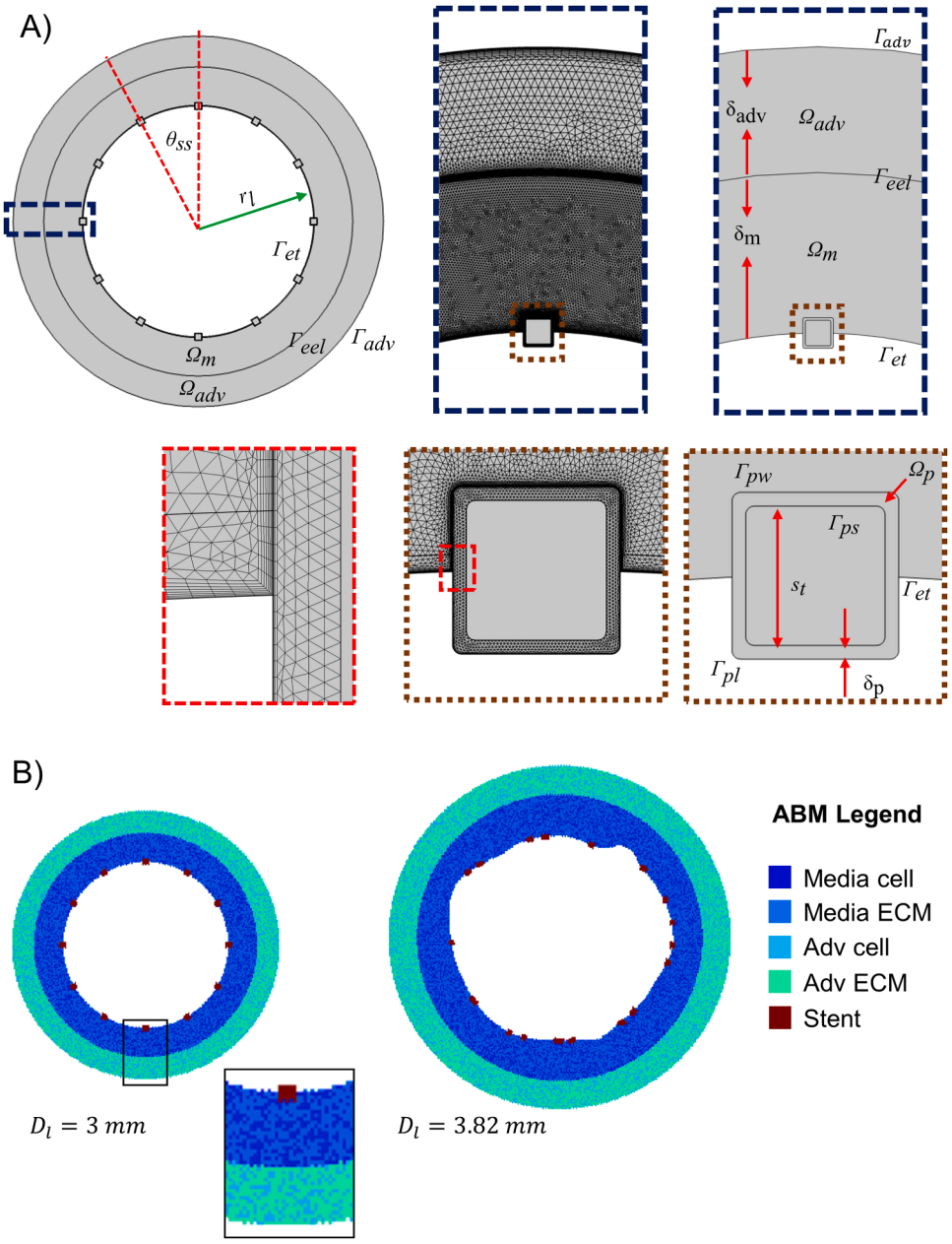

Fig. 3. A) Drug transport model domains and mesh. Idealized coronary artery cross-section with schematic of the domains (Ω), boundaries (Γ) and geometric parameters, and representation of the finite element mesh on magnified portions of the geometry. B) Agent-based model of the idealized (left) and patient-specific (right) coronary artery cross-section, with a magnification on a portion of the arterial wall.

drug, meaning that the higher RS_{ABM} the more cell mitosis is reduced, up to ceasing if $RS_{ABM} = 1$, as defined in the probability equations of $p^h_{division}$ in the media detailed in Table 3. The parameters were tuned to reproduce ~20/25% degree of restenosis at 1-month in the absence of drug [27] and to guarantee a final intimal ECM/SMC ratio (normalized by the initial value) within the range [0.5 1.5], as in [12–14]. SMC mitosis and ECM production determined agent generation, while SMC apoptosis and ECM degradation determined agent removal. In both cases, tissue reorganization was implemented as in [23], being inward- and outward-orientated in the media and in the adventitia, respectively. This implied that growth of the media (*i.e.*, the only layer affected by perturbed agent activities) resulted in lumen narrowing. Regularization processes were performed to guarantee smooth contours [12–14].

Due to the ABM stochasticity, each simulation was repeated three times, and the one with the output minimizing the root mean square deviation of the lumen contour from the average one was selected as the representative condition, and shown [12–14,23].

2.1.3. *Coupling scheme: drug transport and tissue remodelling*

In the two-way coupling case, the nodal lumen, lamina and external border coordinates of the selected ABM output cross-section (from the three repeated simulations) were re-scaled (according to the scaling factor of 25 μm/ABM site) and exported in Rhinoceros (Robert McNeel & Associates), where, through the interpolation of the point coordinates, the remodelled geometry was generated and input into the drug transport module to compute drug transport and update the RS_{ABM} input to cellular activities. Thus, the updated geometry was imported into COMSOL Multiphysics, where a new mesh was discretized. Then at t=coupling time, the transport model was initialized by imposing (i) the RS condition of the last time step of the previous simulation in the media and (ii) either RS=1 or RS=0 within the neointima. The boundary conditions detailed above (Table 2) were applied.

Table 1
Drug transport model equations.

Polymer (Ω_p)	$\frac{\partial c_p}{\partial t} = D_p \nabla^2 c_p, \quad c_p^0 = \frac{M^0}{V_p}$
Media (Ω_m)	$\boldsymbol{u}_m = \frac{K_m}{\mu_p} \nabla p_m, \ \nabla \cdot \boldsymbol{u}_m = 0$
	$\frac{\partial c_m}{\partial t} + \frac{\gamma_m}{\phi_m} \boldsymbol{u}_m \cdot \nabla c_m = \nabla \cdot (\boldsymbol{D}_m \nabla c_m) - \frac{\partial b^s}{\partial t} - \frac{\partial b^{ns}}{\partial t}$
	$\frac{\partial b^s}{\partial t} = k_{on}^s c_m (b_{max}^s - b^s) - k_{off}^s b^s, \qquad b^s(t=0) = 0$
	$\frac{\partial b^{ns}}{\partial t} = k_{on}^{ns} c_m (b_{max}^{ns} - b^{ns}) - k_{off}^{ns} b^{ns}, \qquad b^{ns}(t=0) = 0$
	$RS_{map} = \frac{b^s}{b_{max}^s}; \ RS_{curve} = \frac{1}{V_w} \int_{Vw} \frac{b^s}{b_{max}^s} \, dV_w$
Adventitia (Ω_a)	$\boldsymbol{u}_a = \frac{K_a}{\mu_p} \nabla p_a, \ \nabla \cdot \boldsymbol{u}_a = 0$
	$\frac{\partial c_a}{\partial t} + \frac{\gamma_a}{\phi_a} \boldsymbol{u}_a \cdot \nabla c_a = \nabla \cdot (\boldsymbol{D}_a \nabla c_a)$

c_p: drug concentration in the polymer; D_p: effective polymer coating diffusion coefficient; c_p^0: initial drug concentration in the polymer; M^0: initial mass of drug; V_p: volume of the coating per strut; $\boldsymbol{u}_m$: transmural velocity in the media; K_m: Darcy permeability in the media; μ_p: plasma dynamic viscosity; p_m: pressure field in the media; c_m: dissolved drug concentration in the media; γ_m: hindrance coefficient in the media; ϕ_m: media porosity; $\boldsymbol{D_m}$: diffusivity tensor of the media; b^s: concentration of specifically bound drug; k_{on}^s: specific binding on rate; k_{off}^s: specific binding off rate; b_{max}^s: specific binding site maximum density; b^{ns}: concentration of non-specifically bound drug; k_{on}^{ns}: non-specific binding on rate; k_{off}^{ns}: non-specific binding off rate; b_{max}^{ns}: non-specific binding site maximum density; RS_{map}: spatial contour of receptor saturation (RS) at a specific time instant; RS_{curve}: time-varying mean RS over space; V_w: arterial wall volume; $\boldsymbol{u}_a$: transmural velocity in the adventitia; K_a: Darcy permeability in the adventitia; p_a: pressure field in the adventitia; c_a: dissolved drug concentration in the adventitia; γ_a: hindrance coefficient in the adventitia; ϕ_a: adventitia porosity; $\boldsymbol{D_a}$: diffusivity tensor of the adventitia. The values and references of all the parameters are provided in the Supplementary Table 1.

Table 2
Drug transport model boundary conditions.

Boundary	Condition
Polymer coating-strut interface (Γ_{ps})	Zero-flux [18]
Polymer coating-lumen interface (Γ_{pl})	Infinite sink [18]
Endothelium (Γ_{et})	Infinite sink [10]
Polymer coating-wall interface (Γ_{pw})	Infinite sink [10,18]
External elastic lamina (EEL) (Γ_{eel})	Kedem-Katchalsky [10]
Perivascular edge (Γ_{adv})	Infinite sink [10,18]

Table 3
Agent-based model probability equations.

Media	$p_{division}^h = (\alpha_1 + \alpha_2 I^h)(1 - \alpha_3 RS_{ABM}^h)$
	$p_{apoptosis}^h = \alpha_1$
	$p_{ECMproduction}^h = \alpha_4 + \alpha_5 I^h$
	$p_{ECMdegradation}^h = \frac{\alpha_4}{\beta_{med}}$
Adventitia	$p_{division}^h = p_{apoptosis}^h = \alpha_1$
	$p_{ECMproduction}^h = \beta_{adv} \cdot p_{ECMdegradation}^h = \alpha_4$

$p_{division}^h$: probability of cell mitosis; $p_{apoptosis}^h$: probability of cell apoptosis; $p_{ECMproduction}^h$: probability of extracellular matrix (ECM) production; $p_{ECMdegradation}^h$: probability of ECM degradation; I: inflammatory input; RS_{ABM}: receptor saturation input; α_1, α_2, α_3, α_4, α_5, β_{med}, β_{adv}: parameters driving agent probabilities.

Table 4
Agent-based model parameters.

Parameter	α_1	α_2	α_3	α_4	α_5	βmed	βadv
Value	0.0025	0.025	1	0.0004	0.0125	1.55	2.5

2.2. Studies

Three studies were performed to investigate the impact of different settings/scenarios on ISR: Study 1, the effect of different DM and RP; Study 2, the effect of one-way *vs.* two-way coupling; Study 3, the effect of RS_{map} *vs.* RS_{curve} outputs from the drug transport module to compute RS_{ABM} . Studies 1 and 2 were performed by considering RS_{curve} and the idealized geometry, while Study 3 considered RS_{curve} and RS_{map} and the patient-specific geometry. A detailed description of the various scenarios is provided below.

2.2.1. Study 1

Study 1 applied the one-way coupled framework on the idealized geometry up to 1-month. The drug transport module simulated six different scenarios by imposing different DM and polymer diffusion coefficient D_p (influencing the RP), detailed in Table 5. Six RS_{curve} over 1-month were obtained as output of the six scenarios from the drug transport module and used to initialize the ABM.

2.2.2. Study 2

Study 2 applied the two-way coupled framework on the idealized geometry up to 1-month. The impact of two-way coupling on sA and sD was investigated, these representing extreme scenarios. Specifically, four coupling cases were considered (Table 6). Two coupling times (3 *vs.* 1 days) were investigated, as well as two RS initial conditions within the drug transport module (RS=1 *vs.* RS=0 within the neointima at *t*=coupling time), leading to the following coupling conditions (*i.e.*, C1: 3 days and RS=1, C2: 3 days and RS = 0 and C3: 1 day and RS = 1). For each case, RS_{curve} over the coupling period was computed by the drug transport module and used to initialize the ABM.

2.2.3. Study 3

Study 3 applied the one-way coupled framework to the patient-specific geometry up to 1-month, to study the impact of homogeneous *vs.* heterogeneous RS_{ABM}, obtained from RS_{curve} *vs.* RS_{map}, respectively. The study was performed considering sD. The patient-specific geometry exhibited an irregular and non-symmetric geometry with unequal strut spacing, enabling consideration of the potential differences between RS_{curve} and RS_{map}, compared to the idealized geometry.

3. Results

3.1. Study 1

Fig. 4A displays RS_{curve} computed from the drug transport module under the six scenarios. The variation in DM influenced both the maximum RS achieved and the time-to-peak. With high, mid-high and mid-low DM (sA, sB and sC, respectively) RS~1 was achieved by 2, 4 and

Table 5
Scenarios of study 1.

Scenario	DM [μg/cm^2]	D_p [m^2/s]
sA	100	1×10^{-17}
sB	10	1×10^{-17}
sC	2.5	1×10^{-17}
sD	1	1×10^{-17}
sE (Fast)	2.5	1×10^{-16}
sF (Slow)	2.5	1×10^{-18}

DM: drug mass; D_p: effective polymer coating diffusion coefficient.

Table 6
Coupling cases of study 2.

Coupling case	Coupling time	Initial condition
sA–C1	3 days	RS=1
sD–C1	3 days	RS=1
sD–C2	3 days	RS=0
sD–C3	1 day	RS=1

RS: receptor saturation.

8 days, respectively, while with low DM (sD) a maximum RS=0.93 was achieved around day 23. Moreover, while in sA, RS∼1 was maintained up to 1-month, in sB, sC and sD, a slight decrease in RS was observed. The variation of RP influenced the rate of increase of RS and, consequently, the maximum RS achieved within 1-month. With a mid-low DM, a fast RP (sE) determined a fast initial rate of RS, with a peak of RS∼1 around day 4, decreasing to RS=0.8 at day 30, and a slow RP (sF) determined a slow initial rate of RS, with a peak of RS∼0.92 at day 30.

The different scenarios displayed varying arterial responses (Fig. 4B). In the absence of drug, a ∼30% lumen area reduction at 1-month was obtained. Drug release halved the lumen area reduction (to ∼13/17% at 1-month) in sA, sB, sC and sE. A moderate improvement in outcome with a 22/24% lumen area reduction at 1-month was obtained with sD and sF, respectively. In the low-restenosis scenarios sA, sB, sC and sE, a slight decrease in SMC content was observed due to inhibited SMC proliferation, while SMC apoptosis still occurred. Thus, in sA, sB, sC and sE drug efficacy was maximum and the lumen area reduction over 1-month was solely attributed to increased ECM production. In the moderate-restenosis scenarios sD and sF, SMC remained stable over time, resulting in higher availability of SMCs producing ECM, compared to the previous scenarios. Consequently, the lumen area decrease over 1-month was attributable to the net increase in ECM content, higher than in sA, sB, sC and sE due to the greater content of synthetic SMCs. In all scenarios, the adventitia remodelled without experiencing changes in cell/ECM content and area. Fig. 5 depicts the ABM cross-sections at days 15 and 30 for the six scenarios. As expected, the ABM simulated a homogeneous growth, due to the uniform RS_{ABM} input.

3.2. Study 2

The effect of the two-way coupling was analysed both at the drug transport module and tissue remodelling module levels. At the drug transport module level, the two-way coupling did not affect the RS_{curve} over 1-month in sA (sA *vs.* sA–C1), while it influenced the RS_{curve} over 1-month in sD in all the cases (sD *vs.* sD–C1, sD–C2 and sD–C3) (Fig. 6A). Specifically, when considering RS=1 in the neointima, both the 3-day (sD–C1) and 1-day (sD–C3) coupling led to a faster RS increase, with a peak of RS=0.96 at day 15, compared to the RS=0.93 at day 23 (sD). Differently, when considering RS=0 in the neointima (sD–C2) at each coupling time, RS dropped below its prior level due to increase in the area with RS=0. This led to decreased drug efficacy compared to the one-way coupling case (sD).

At the tissue remodelling module level, as expected from the analysis of RS_{curve}, a minor difference was obtained between the one-way and two-way coupling in sA (sA *vs.* sA–C1), with the two-way coupling presenting a slight decrease of restenosis at 1-month (Fig. 6B). Notably, despite the non-negligible changes in RS_{curve} of sD between the one-way and the two-way coupling (sD *vs.* sD–C1, sD–C2, and sD–C3), a minor difference was observed in the 1-month restenosis degree (Fig. 6B). Fig. 6C shows the ABM cross-sections at days 15 and 30 for the four coupling cases. In all cases, homogeneous growth was observed. Moreover, as expected from the lumen area trend (Fig. 6B), negligible differences in output cross-sections were obtained between the one-way and two-way couplings (Fig. 5 *vs.* 6C).

3.3. Study 3

Fig. 7A-B depict, respectively, the RS_{curve} and RS_{map} over time, computed by the drug transport module. No differences in the lumen area over time were observed between RS_{curve} *vs.* RS_{map} cases (Fig. 7C). This was in line with expectations since RS_{curve} represented the average over space of RS_{map}, at each time-instant. Thus, from a quantitative perspective, the overall effect on SMCs was similar. Fig. 7D shows the ABM cross-sections at days 15 and 30 for RS_{curve} and RS_{map} cases. Minor

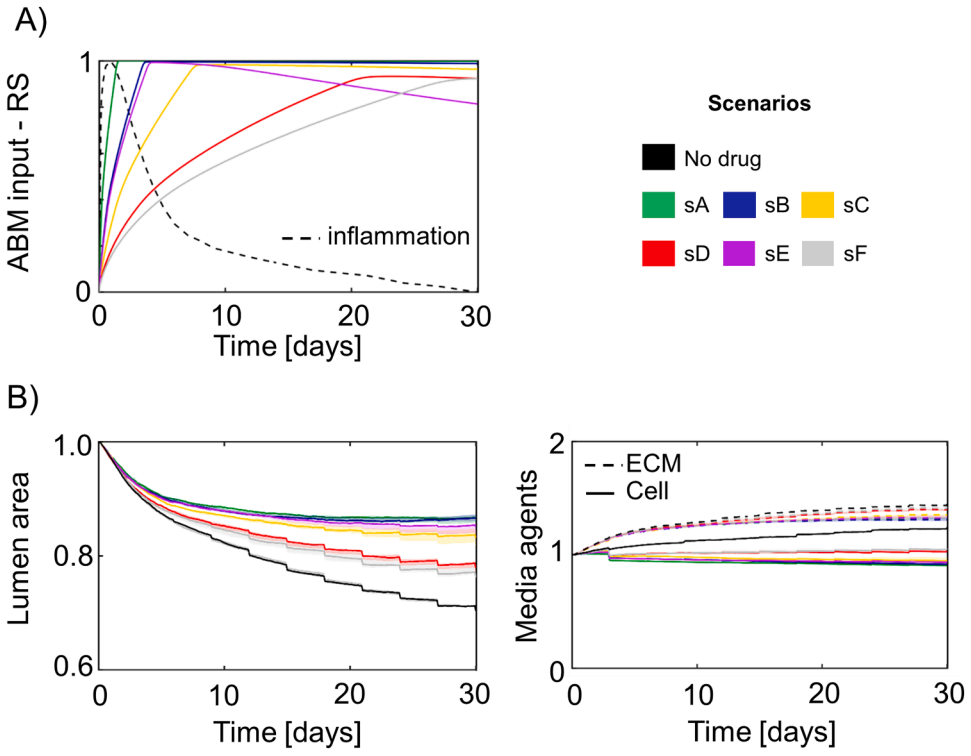

Fig. 4. Results of study 1. A) Receptor saturation (RS) over time computed by the drug transport module for the scenarios sA (green), sB (blue), sC (yellow), sD (red), sE (violet) and sF (grey) and inflammatory curve (dashed black line). B) Normalized lumen area (left) and normalized extracellular matrix (ECM) and cell medial content over time (right) obtained from the tissue remodelling module for the six scenarios sA (green), sB (blue), sC (yellow), sD (red), sE (violet) and sF (grey) and for the case without drug (black), represented as median and interquartile range.

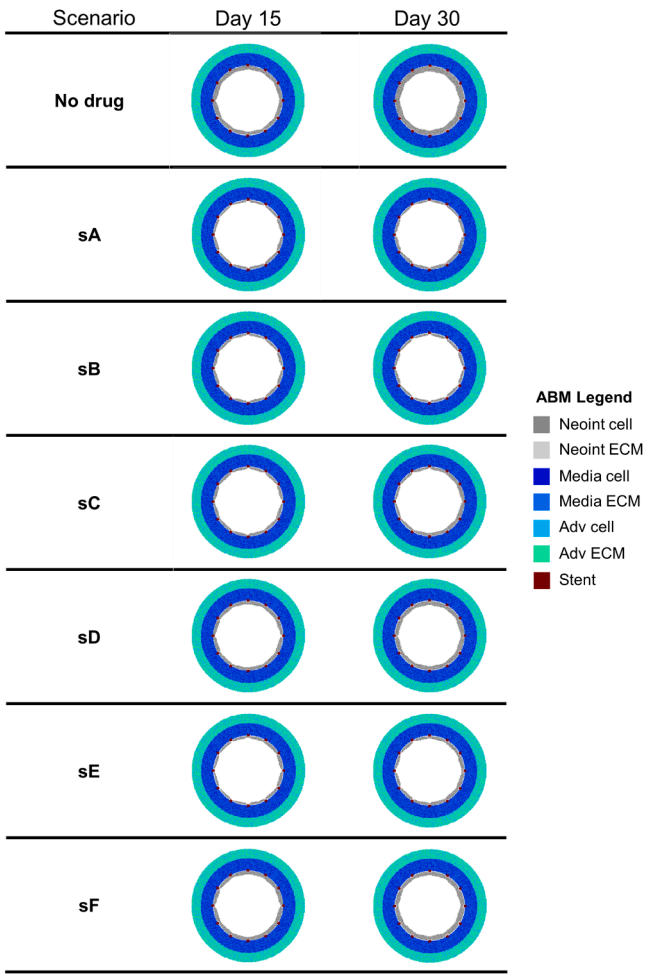

Fig. 5. Results of study 1. Agent-based model (ABM) cross-sections at day 15 and day 30 for the case without drug and the six scenarios of study 1 (sA, sB, sC, sD, sE, sF). For each scenario, the results were retrieved from one out of three ABM simulations, namely the one presenting the lumen configuration minimizing the root mean square deviation from the average one.

differences in the ABM growth pattern were found at day 15 between the two cases, but attenuated over time, vanishing by day 30.

4. Discussion

A novel multiscale framework was developed in which spatiotemporal drug transport simulations were coupled with an ABM of cellular dynamics to investigate the effect of drug release on ISR at the cell-tissue scale. To date, it appears only two ABMs included the effect of drug release on ISR [7,28]. In those frameworks, the drug transport module comprised simple steady diffusion of free drug and neglected binding kinetics. In the present work, a more sophisticated drug transport model was adopted and a multiscale framework was implemented to simulate the bi-directional interaction between spatiotemporal drug release and tissue remodelling. Recently, McQueen et al. [11] proposed a similar, but fully-continuum, approach, where SMC and ECM dynamics were modelled through partial differential equations and drug release was computed simultaneously with changes in cellular and extracellular content. However, tissue growth was computed at the end of the simulation based on mass balance derived from cellular dynamics, meaning that the drug release was de-coupled from the morphological and volumetric change. Differently, in the present framework the arterial wall remodelling occurred simultaneously with the cellular dynamics and, when two-way coupling was considered, the influence of the geometrical change on the drug release was considered by solving drug transport in the deformed geometry at each coupling time.

Three studies were performed to investigate different scenarios in terms of DM, RP, coupling schemes and arterial geometries. As expected, increased DM and fast RP led to a quicker and greater RS peak, resulting in a smaller degree of restenosis, compared to low DM and slow RP scenarios. However, the ABM was not sensitive to small translations in time of the RS peak, if the RS peak occurred by 5 days, as demonstrated by the responses in sA and sB (Fig. 4). Moreover, a decay of RS following day 5 did not impact the ABM response largely, as demonstrated by the small differences in the ISR severity obtained in sB *vs.* sE (Fig. 4). Additionally, the ABM was not sensitive to changes in the RS_{curve} of sD between the one-way and two-way coupling (Fig. 6). The lack of remarkable differences in the simulated ISR, despite differences in RS_{curves}, was probably due to the assumed inflammatory input, which presented an early peak and lost most of its effect after day 5 (I<0.4). Thus, RS_{curve} within the first 5 days mainly governed the ABM output, while changes in RS_{curve} after day 5 had negligible effects on the final ISR. Finally, a series of factors determined the lack of remarkable spatial heterogeneity in the RS_{map} case of Study 3: (i) the lumen geometry and stent strut distribution was not extremely heterogeneous; (ii) uniform tissue layer properties were considered; (iii) the selected scenario sD led to a condition in which up to day 5 (when the inflammation lost most of its effect) more than 50% of the media and especially the outer ring of the media presented RS=0, thus determining a uniformly distributed growth; (iv) the drug only affected SMC proliferation but not ECM production, thus uniform ECM production further mitigated the potential heterogeneity deriving from SMC proliferation; (v) after day 20, the growth ceased due to the low influence of the inflammation, together with the high RS and the lumen border regularized due to the application of smoothing algorithms.

Overall, the three studies demonstrated the versatility and proof-of-concept of the framework, which enables analyses with (i) one-way or two-way coupling, (ii) RS_{curve} or RS_{map} inputs and (iii) idealized or patient-specific geometries. Study 1 highlighted that a small DM combined with fast RP determine a similar ISR degree as a high DM and moderate RP, suggesting scope for optimizing DES design. The studies also shed light on the effects that the assumed inflammatory input has on the ABM output and on deciphering the interaction between drug release and remodelling. In particular, with the assumed inflammatory curve (abrupt and sharp), the long-term (*i.e.*, after the first 5 days) drug release does not have a notable impact on SMC proliferation. Differently, in case sustained inflammatory curves were considered, the entire RS profile would have probably influenced cellular dynamics and restenosis. In this context, a sensitivity analysis of the inflammatory input should be performed in future to investigate the ABM working mechanisms.

This study served as proof-of-concept and was not exempt from limitations. First, a 2D geometry was considered. In future, a combined 3D-2D approach can be applied as has been done in previous studies [12–14,23,24], in which the continuum-based module (the drug transport module in this case) is solved in a 3D geometry and the discrete-based module (the tissue remodelling module) is solved at selected stented vessel cross-sections. Second, a simplified approach was adopted to simulate the restenosis trigger, consisting of a spatially uniform, time-varying inflammatory curve. Inflammatory cells and their drug receptors were not explicitly modelled. Thus, the interaction between drug and inflammatory cells was neglected, although such interactions could have implications in terms of drug efficacy. Moreover, thanks to the modularity of the framework, stent expansion and hemodynamic modules can be included, allowing computation of the intervention-induced damage and perturbed fluid-dynamics, which were used as the restenosis driver in previous works [12–14]. Third, the drug transport properties of the neointimal tissue were assumed to be identical to those in the media layer, although in reality these may differ due to differences in composition between the two regions. Herein, a

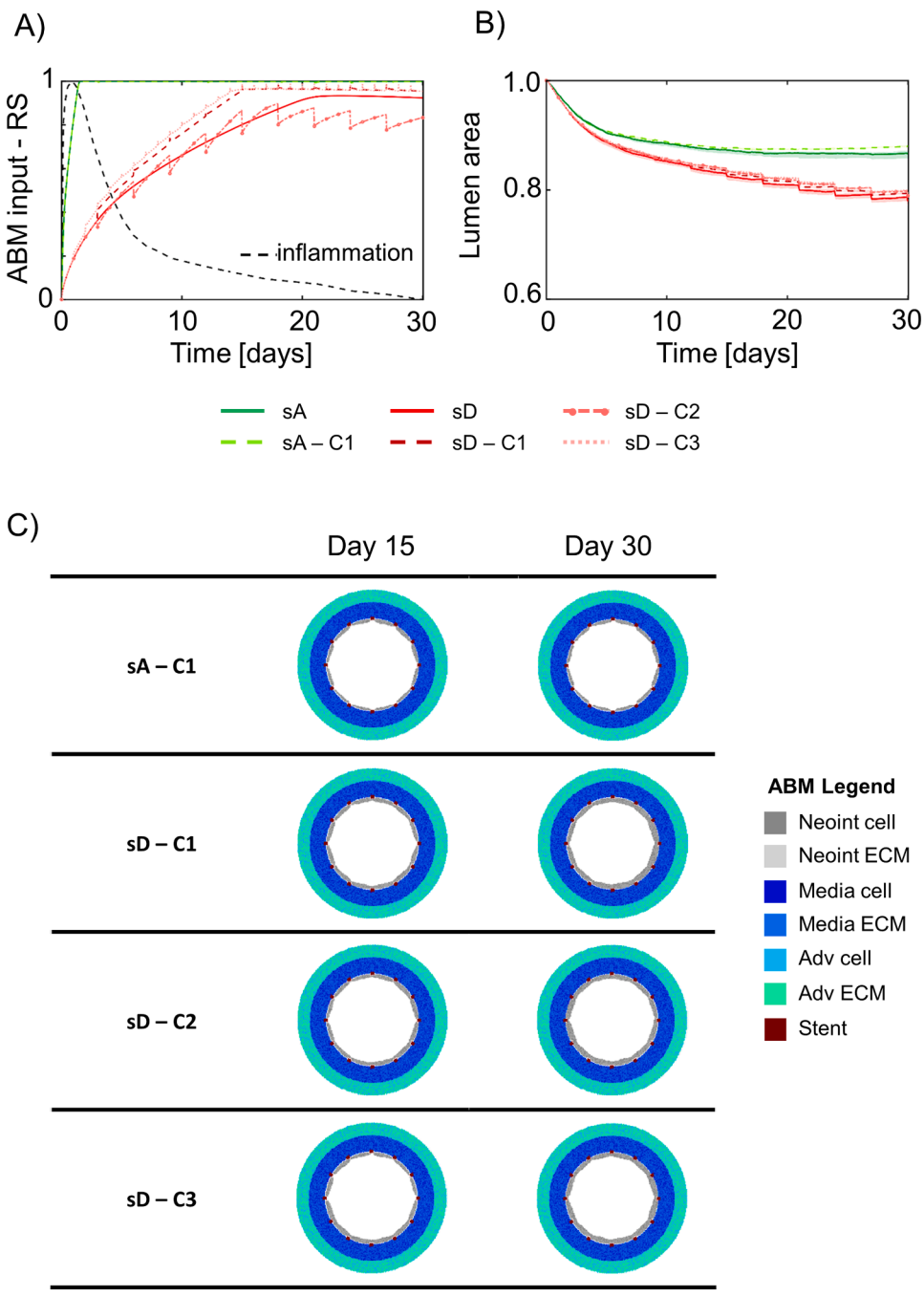

Fig. 6. Results of study 2. A) Receptor saturation (RS) over time computed by the drug transport module for the scenarios sA (green – solid line) and sD (red – solid line) and their corresponding coupling cases, namely sA – C1 (green – dashed line), sD – C1 (red – dashed line), sD – C2 (red – dash-dotted line) and sD – C3 (red – dotted line). Representation of the inflammatory curve (dashed black line). B) Normalized lumen area over time (median and interquartile range) obtained from the tissue remodelling module for the scenarios sA (green – solid line) and sD (red – solid line) and their corresponding coupling cases, namely sA – C1 (green – dashed line), sD – C1 (red – dashed line), sD – C2 (red – dash-dotted line) and sD – C3 (red – dotted line). C) Agent-based model (ABM) cross-sections at day 15 and day 30 for the coupling cases sA – C1, sD – C1, sD – C2 and sD – C3. For each case, the results were retrieved from one out of three ABM simulations, namely the one presenting the lumen configuration minimizing the root mean square deviation from the average one.

homogeneous arterial wall tissue was assumed, although different tissue and plaque composition is thought to markedly impact on drug release, retention in tissue and, consequently, the arterial remodelling response. Future research should focus on considering arterial tissue heterogeneity, thus providing a more accurate drug transport model.

Finally, the feasibility of the idealized to patient-specific translation was demonstrated by applying the framework to a realistic geometry. In this context, future steps will address the framework calibration and validation. To this aim, the pipeline adopted in the previously proposed ISR studies [12,14] can be applied herein, consisting of: (i) a preliminary sensitivity analysis to identify the driving ABM parameters, (ii) a combined surrogate modelling – genetic algorithm optimization approach to calibrate the driving ABM parameters based on the patient outputs and (iii) the application of the calibrated framework to a different patient case to validate it.

5. Conclusions

A novel multiscale framework coupling drug kinetics with an ABM of arterial wall remodelling has been presented. The work demonstrated the suitability of the framework to investigate the multiscale and multifactorial mechanisms underlying arterial wall remodelling following DES implantation. The results highlighted that the ISR degree emerged from the interplay between the inflammatory response and RS trend, in turn driven by DM and RP. In particular, with an abrupt inflammatory response the RS within the first 5 post-operative days mainly governed the ISR degree, thus a sustained drug release over an entire month may not be necessary. The proof-of-concept application to patient-specific geometries lays the foundations for future research in the field, including its calibration and validation on patient datasets and the investigation of the effects of different plaque composition on the

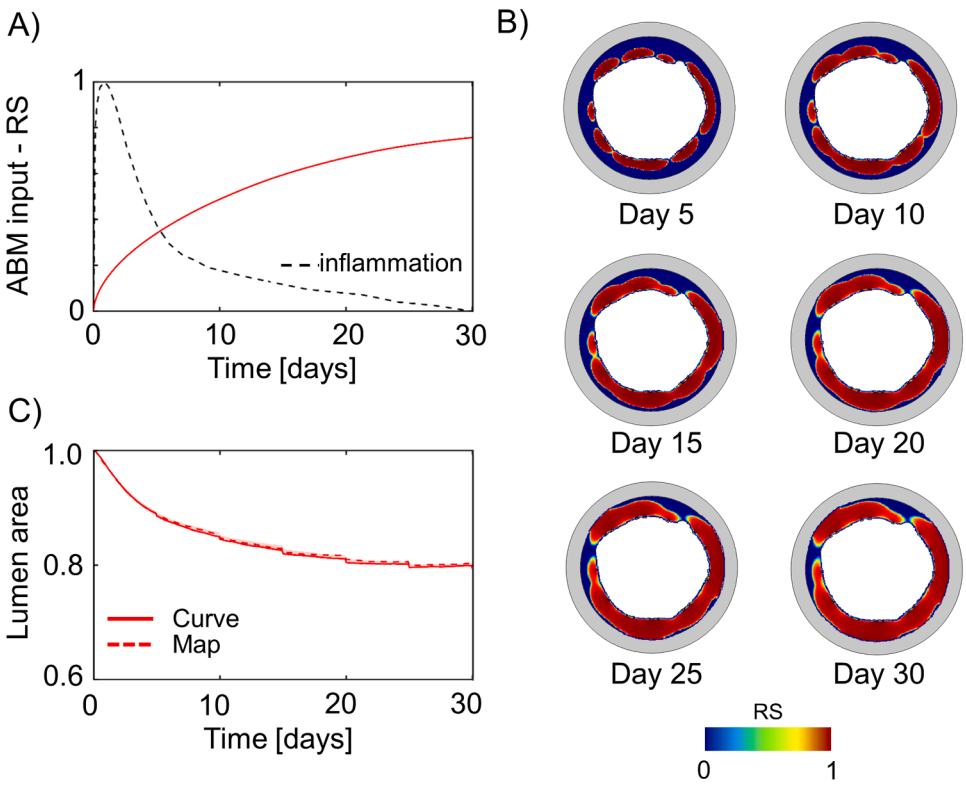

Fig. 7. Results of study 3. A) Receptor saturation (RS) over time for the patient-specific arterial geometry (considering scenario sD), computed by the drug transport module, and representation of the inflammatory curve (dashed black line). B) RS map at day 5, 10, 15, 20, 25 and 30 computed by the drug transport module. C) Normalized lumen area over time (median and interquartile range) obtained from the tissue remodelling module for the curve case (*i.e.*, the RS input was the RS curve over time) and map case (*i.e.*, the RS input was the RS map over time). D) Agent-based model (ABM) cross-sections at day 15 and day 30 for the curve and map cases. For each case, the results were retrieved from one out of three ABM simulations, namely the one presenting the lumen configuration minimizing the root mean square deviation from the average one.

arterial response to DES. Finally, the framework developed is not only applicable to DES and may be tailored to any scenario where the influence of drug delivery on tissue remodelling post device deployment is of interest.

Data accessibility

All data supporting this study are provided within the main text.

Funding

SM and FM acknowledge funding provided by EPSRC (grant number EP/S030875/1).

Declaration of Competing Interest

The authors declare that they have no conflict of interest.

Supplementary materials

Supplementary material associated with this article can be found, in the online version, at doi:10.1016/j.cmpb.2023.107739.

References

[1] S.S. Virani, A. Alonso, H.J. Aparicio, E.J. Benjamin, M.S. Bittencourt, C. W. Callaway, A.P. Carson, A.M. Chamberlain, S. Cheng, F.N. Delling, M.S. V Elkind, K.R. Evenson, J.F. Ferguson, D.K. Gupta, S.S. Khan, B.M. Kissela, K.L. Knutson, C. D. Lee, T.T. Lewis, J. Liu, M.S. Loop, P.L. Lutsey, J. Ma, J. Mackey, S.S. Martin, D. B. Matchar, M.E. Mussolino, S.D. Navaneethan, A.M. Perak, G.A. Roth, Z. Samad, G.M. Satou, E.B. Schroeder, S.H. Shah, C.M. Shay, A. Stokes, L.B. VanWagner, N. Y. Wang, C.W. Tsao, Heart disease and stroke statistics-2021 update: a report from the American Heart Association, Circulation 143 (2021) e254–e743, https://doi.org/10.1161/CIR.0000000000000950.

[2] F. Alfonso, J.J. Coughlan, D. Giacoppo, A. Kastrati, R.A. Byrne, Management of in-stent restenosis, EuroIntervention J. Eur. Collab. with Work. Gr. Interv. Cardiol. Eur. Soc. Cardiol. 18 (2022) e103–e123, https://doi.org/10.4244/EIJ-D-21-01034.

[3] E. Shlofmitz, M. Iantorno, R. Waksman, Restenosis of drug-eluting stents, Circ. Cardiovasc. Interv. 12 (2019), e007023, https://doi.org/10.1161/CIRCINTERVENTIONS.118.007023.
[4] J. Aoki, K. Tanabe, Mechanisms of drug-eluting stent restenosis, Cardiovasc. Interv. Ther. 36 (2021) 23–29, https://doi.org/10.1007/s12928-020-00734-7.
[5] A. McQueen, J. Escuer, A. Aggarwal, S. Kennedy, C. McCormick, K. Oldroyd, S. McGinty, Do we really understand how drug eluted from stents modulates arterial healing? Int. J. Pharm. 601 (2021), 120575 https://doi.org/10.1016/j.ijpharm.2021.120575.
[6] A. Corti, M. Colombo, F. Migliavacca, J.F. Rodriguez Matas, S. Casarin, C. Chiastra, Multiscale computational modeling of vascular adaptation: a systems biology approach using agent-based models, Front. Bioeng. Biotechnol. 9 (2021), 744560, https://doi.org/10.3389/fbioe.2021.744560.
[7] A. Caiazzo, D. Evans, J.L. Falcone, J. Hegewald, E. Lorenz, B. Stahl, D. Wang, J. Bernsdorf, B. Chopard, J. Gunn, R. Hose, M. Krafczyk, P. Lawford, R. Smallwood, D. Walker, A. Hoekstra, A complex automata approach for in-stent restenosis: two-dimensional multiscale modelling and simulations, J. Comput. Sci. 2 (2011) 9–17, https://doi.org/10.1016/j.jocs.2010.09.002.
[8] H. Tahir, C. Bona-Casas, A.G. Hoekstra, Modelling the effect of a functional endothelium on the development of in-stent restenosis, PLoS One 8 (2013) e66138, https://doi.org/10.1371/journal.pone.0066138.
[9] J. Escuer, M. Cebollero, E. Peña, S. McGinty, M.A. Martínez, How does stent expansion alter drug transport properties of the arterial wall? J. Mech. Behav. Biomed. Mater. 104 (2020), 103610 https://doi.org/10.1016/j.jmbbm.2019.103610.
[10] J. Escuer, A.F. Schmidt, E. Peña, M.A. Martínez, S. McGinty, Mathematical modelling of endovascular drug delivery: balloons *versus* stents, Int. J. Pharm. 620 (2022), 121742, https://doi.org/10.1016/j.ijpharm.2022.121742.
[11] A. McQueen, J. Escuer, A.F. Schmidt, A. Aggarwal, S. Kennedy, C. McCormick, K. Oldroyd, S. McGinty, An intricate interplay between stent drug dose and release rate dictates arterial restenosis, J. Control. Release Off. J. Control. Release Soc. 349 (2022) 992–1008, https://doi.org/10.1016/j.jconrel.2022.07.037.
[12] A. Corti, M. Colombo, J.M. Rozowsky, S. Casarin, Y. He, D. Carbonaro, F. Migliavacca, J.F. Rodriguez Matas, S.A. Berceli, C. Chiastra, A predictive multiscale model of in-stent restenosis in femoral arteries: linking hemodynamics and gene expression with an agent-based model of cellular dynamics, J. R. Soc. Interface. (2022), 20210871, https://doi.org/10.1098/rsif.2021.0871.
[13] A. Corti, M. Colombo, F. Migliavacca, S.A. Berceli, S. Casarin, J.F. Rodriguez Matas, C. Chiastra, Multiscale agent-based modeling of restenosis after percutaneous transluminal angioplasty: effects of tissue damage and hemodynamics on cellular activity, Comput. Biol. Med. 147 (2022), 105753, https://doi.org/10.1016/j.compbiomed.2022.105753.
[14] A. Corti, F. Migliavacca, S.A. Berceli, C. Chiastra, Predicting 1-year in-stent restenosis in superficial femoral arteries through multiscale computational modelling, J. R. Soc. Interface 20 (2023), 20220876, https://doi.org/10.1098/rsif.2022.0876.
[15] C. Chiastra, S. Migliori, F. Burzotta, G. Dubini, F. Migliavacca, Patient-specific modeling of stented coronary arteries reconstructed from optical coherence tomography: towards a widespread clinical use of fluid dynamics analyses, J. Cardiovasc. Transl. Res. 11 (2018) 156–172, https://doi.org/10.1007/s12265-017-9777-6.
[16] C. Chiastra, G. Dubini, F. Migliavacca, Chapter 11 - Hemodynamic perturbations due to the presence of stents, in: J. Ohayon, G. Finet, R.I. Pettigrew (Eds.), Biomech. Coron. Atheroscler. Plaque, Academic Press, 2021, pp. 251–271, https://doi.org/10.1016/B978-0-12-817195-0.00011-1.
[17] J. Escuer, I. Aznar, C. McCormick, E. Peña, S. McGinty, M.A. Martínez, Influence of vessel curvature and plaque composition on drug transport in the arterial wall following drug-eluting stent implantation, Biomech. Model. Mechanobiol (2021), https://doi.org/10.1007/s10237-020-01415-3. In press.
[18] F. Bozsak, J.M. Chomaz, A.I. Barakat, Modeling the transport of drugs eluted from stents: physical phenomena driving drug distribution in the arterial wall, Biomech. Model. Mechanobiol. 13 (2014) 327–347, https://doi.org/10.1007/s10237-013-0546-4.
[19] A.R. Tzafriri, A. Groothuis, G.S. Price, E.R. Edelman, Stent elution rate determines drug deposition and receptor-mediated effects, J. Control. Release. 161 (2012) 918–926, https://doi.org/10.1016/j.jconrel.2012.05.039.
[20] S. McGinty, A decade of modelling drug release from arterial stents, Math. Biosci. 257 (2014) 80–90, https://doi.org/10.1016/j.mbs.2014.06.016.
[21] A.R. Tzafriri, F. Garcia-Polite, X. Li, J. Keating, J.M. Balaguer, B. Zani, L. Bailey, P. Markham, T.C. Kiorpes, W. Carlyle, E.R. Edelman, Defining drug and target protein distributions after stent-based drug release: durable *versus* deployable coatings, J. Control. Release Off. J. Control. Release Soc. 274 (2018) 102–108, https://doi.org/10.1016/j.jconrel.2018.02.007.
[22] H. Tahir, I. Niculescu, C. Bona-Casas, R.M.H. Merks, A.G. Hoekstra, An *in silico* study on the role of smooth muscle cell migration in neointimal formation after coronary stenting, J. R. Soc. Interface 12 (2015), 20150358, https://doi.org/10.1098/rsif.2015.0358.
[23] A. Corti, C. Chiastra, M. Colombo, M. Garbey, F. Migliavacca, S. Casarin, A fully coupled computational fluid dynamics – agent-based model of atherosclerotic plaque development: multiscale modeling framework and parameter sensitivity analysis, Comput. Biol. Med. 118 (2020), 103623, https://doi.org/10.1016/j.compbiomed.2020.103623.
[24] A. Corti, S. Casarin, C. Chiastra, M. Colombo, F. Migliavacca, M. Garbey, et al., A multiscale model of atherosclerotic plaque development: toward a coupling between an agent-based model and CFD simulations, in: J.M.F. Rodrigues, P.J.S. Cardoso, J. Monteiro, R. Lam, V. V Krzhizhanovskaya, M.H. Lees (Eds.), et al., Proceedings of the Comput. Sci. – ICCS 2019, Cham, Springer International Publishing, 2019, pp. 410–423, https://doi.org/10.1007/978-3-030-22747-0_31.
[25] M. Schillinger, M. Exner, W. Mlekusch, H. Rumpold, R. Ahmadi, S. Sabeti, M. Haumer, O. Wagner, E. Minar, Vascular inflammation and percutaneous transluminal angioplasty of the femoropopliteal artery: association with restenosis, Radiology 225 (2002) 21–26, https://doi.org/10.1148/radiol.2251011809.
[26] M. Schillinger, M. Exner, W. Mlekusch, M. Haumer, R. Ahmadi, H. Rumpold, O. Wagner, E. Minar, Balloon angioplasty and stent implantation induce a vascular inflammatory reaction, J. Endovasc. Ther. an Off. J. Int. Soc. Endovasc. Spec. 9 (2002) 59–66, https://doi.org/10.1177/152660280200900111.
[27] J. Kotani, M. Awata, S. Nanto, M. Uematsu, F. Oshima, H. Minamiguchi, G. S. Mintz, S. Nagata, Incomplete neointimal coverage of sirolimus-eluting stents: angioscopic findings, J. Am. Coll. Cardiol. 47 (2006) 2108–2111, https://doi.org/10.1016/j.jacc.2005.11.092.
[28] H. Tahir, A.G. Hoekstra, E. Lorenz, P.V. Lawford, D.R. Hose, J. Gunn, D.J.W. Evans, Multi-scale simulations of the dynamics of in-stent restenosis: impact of stent deployment and design, Interface Focus 1 (2011) 365–373, https://doi.org/10.1098/rsfs.2010.0024.